Tailoring IONP shape and designing nanocomposite IONS@GN toward modification of SPCE to enhance electrochemical degradation of organic dye

Materials Research Express

OPEN ACCESS

RECEIVED
5 November 2019

REVISED
6 December 2019

ACCEPTED FOR PUBLICATION
20 December 2019

PUBLISHED
6 January 2020

PAPER

Tailoring IONP shape and designing nanocomposite IONS@GN toward modification of SPCE to enhance electrochemical degradation of organic dye

Miloš Ognjanović[1,4], Dalibor M Stanković[1], Martin Fabián[2], Sanja Vranješ-Đurić[1], Antić Bratislav[1,4] and Biljana Dojčinović[3]

[1] The Vinca Institute of Nuclear Sciences, University of Belgrade, Mike Petrovića Alasa 12-14, 11001 Belgrade, Serbia
[2] Institute of Geotechnics, Slovak Academy of Sciences, Watsonova 45, 04001 Košice, Slovakia
[3] Institute of Chemistry, Technology and Metallurgy, University of Belgrade, Studentski Trg 12-16, 11000 Belgrade, Serbia
[4] Authors to whom any correspondence should be addressed.

E-mail: miloso@vin.bg.ac.rs and bantic@vin.bg.ac.rs

Keywords: iron oxide, graphene, screen-printed electrode, electrochemical degradation, organic dye

Supplementary material for this article is available online

Abstract

Iron oxide nanoparticles (IONP) with different distinctive morphologies (spherical, cubic, flower-like and needles) were utilized for modification of screen-printed carbon electrodes (SPCE) to be used for synthetic organic dye degradation by an electrochemical approach. This platform was implemented for removal of the synthetic organic dye, Reactive Black 5 (RB5) in aqueous solution. Modified SPCE with spherically shaped IONP (IONS) had the highest dye removal efficiency. Thus, IONS were then used for surface decoration of the most common carbon-based materials (graphene, graphene oxide, carboxylated graphene, graphene nanoribbons, graphene nanoplatelets, single- and multi-wall carbon nanotubes), and the nanocomposites formed were deposited on the electrode surfaces. Using IONS/graphene composite (IONS@GN) for electrode modification resulted in the best effect. Removal of RB5 with this electrode was 51% better in comparison with bare SPCE, reducing the time required for complete dye degradation from 61 to 30 min Using IONS-modified SPCE, total RB5 removal occurred in 51 min, improving the performance by 16% over that of bare SPCE. The effects determined, i.e., the best IONP morphology and best type of carbon-based material for nanocomposite formation to enhance RB5 removal will provide guidelines for further modifications of SPCE with nanomaterials and nanocomposites, for application of this electrochemical approach in the degradation of organic pollutants.

1. Introduction

Magnetic nanoparticles (MNP) are one of the most vital and fastest-growing areas of research in the field of nanotechnology. Their properties are significantly modified in comparison with their bulk counterparts and depend on several factors such as composition, shape, size, surface morphology, anisotropy, inter-particle interactions, etc [1–3]. The synthesis of MNP with desired morphology (sphere, cubic, rod, flowers, etc), size, and size distribution has attracted significant attention. Among them, iron oxide nanoparticles (IONP) are of growing interest in different areas of technology, and they are used often as model systems in theoretical investigations. Particularly, magnetite (Fe_3O_4) and maghemite (γ-Fe_2O_3) and their composites are widely studied because of their potential applications in medicine, catalysis, waste-water treatment, biosensors, etc [1–4]. As an example, the use of IONP functionalized with poly(methyl methacrylate) for heavy metal removal (Pb(II), Hg(II), Cu(II), and Co(II)) has been demonstrated, where the high surface-to-volume ratio of the nanoparticles provides high adsorption capacity, and the magnetic nature of nanoparticles enables heavy metal removal using external magnetic fields [2]. The use of magnetic nanoparticles in organic waste treatment is

heavily researched. Recently, magnetic iron cerium bimetal oxides (MMIC) were used as catalyst for oxidation of arsenite [5]. Guo *et al* proposed α-Fe_2O_3/Bi_2WO_6 composite for photocatalytic degradation of organic pollutants under visible light [6], while Zhang *et al* presented results of Fe_2O_3-Pillared Rectorite as a heterogeneous catalyst for photodegradation [7]. Other than this, the use of TiO_2 nanoparticles in catalysis is well known [8–12]

On the other hand, functional, carbon-based nanomaterials are in focus because of the great diversity of their technological and industrial applications. Among the carbon nanomaterials, graphene is the building block of graphitic materials such as carbon nanotubes, carbon nanoribbons, carbon nanoplatelets, fullerenes, graphene oxides, and graphite. Carbonaceous materials are highly electrically conductive materials and, nowadays, are widely exploited in various electrochemistry fields [13–17]. Graphene (GN) is a single atomic layer of sp^2 carbon atoms. This configuration provides the material with extraordinary properties such as large surface area, great electrical conductivity, high mechanical strength, substantial elasticity, and thermal conductivity [18]. Functionalization and dispersion of GN sheets are of crucial importance for their end applications and to prevent the agglomeration of layers of GN, so maintaining GN's inherent properties [19].

Functionalizing GN with carboxyl groups (-COOH) produces carboxylated graphene (cGN), which is used in various fields [20]. Graphene oxide (GO) is synthesized using strong oxidizing agents on GN, resulting in nonconductive hydrophilic carbon-containing oxygen functional groups [21, 22]. Reduced graphene oxide (rGO) is produced from the reduction of GO by thermal, chemical, microwave or electrical treatments [23–25]. Graphene nanoribbons (GNR) are narrow strips of GN or single-layer graphite and are combined to form the structures of carbon nanotubes (CNT) and GN nanosheets (GNS) [26]. Graphene nanoplatelets (GNP) consist of small stacks of GN that are used in many industrial applications, including wastewater treatment [27]. Single-wall and multi-wall carbon nanotubes (SWCNT and MWCNT) have attracted great interest in wastewater treatment due to their large specific surface area, small size, and hollow and layered structure [28, 29]. In very recent years, great effort has been made to treat wastewater with carbonaceous materials (or their composites with IONPs) using an electrochemical approach, which has good potential to deal with many kinds of organic and inorganic wastewater pollutants. As an example, it is worth mentioning that IONP/graphene composites such as Fe_3O_4/r-GO are extremely promising candidates for a wide range of electrochemical sensing and biosensing applications [30].

The treatment of wastewater containing aromatic dyes is difficult because the aromatic structures of the dyes make them highly resistant to light, heat, and oxidizing agents [31, 32]. Recently, a number of processes were proposed in the literature for mitigating dyes and other organic pollutants, and which are based on novel approaches such as use of the dielectric barrier discharge ozone reaction [33], membrane filtration [34], nanofiltration [35], biological treatment [36], and various electrochemical methods [37–39]. Treatments of dyes using electrochemical approaches are mainly focused on electrocoagulation and electrochemical oxidation since electrochemical reduction has the slowest discolouration effect [40]. They can be also combined with photo-assisted degradations (known as photo electro-Fenton reaction). In some cases, electrochemical technologies are the most adequate machinery for dealing with wastewaters containing these pollutant dyes. The main problem with this strategy can be the performance of the electrodes. However, magnetic nanomaterials, both nanoparticles and nanocomposites, with massive specific surface area and small diffusion resistance, have been widely recognized as efficient adsorbents [41, 42].

The main motive of this study was to investigate the influence of the morphology of differently shaped IONPs for azo dye decolourization from aqueous solution. Therefore, iron oxide nanospheres, cubes, flowers, and needles were synthesized and used to modify bare SPCE to enhance the efficiency of dye removal by electrochemical degradation. The morphology with the best performance was then selected for functionalization of the most common carbon materials currently used to further improve the dye removal efficiency. Reactive Black 5 was chosen as a model dye due to its wide application in the textile industry. In line with our goal, the factors affecting dye removal performance, i.e., dosage, pH, supporting electrolyte, applied potential, and dye concentration were studied based on our previous experience. The kinetics of RB5 removal by decorating IONP on top of SPCE was studied. Electrochemical impedance spectroscopy (EIS), along with other techniques such as transmission electron microscopy (TEM), field emission-scanning electron microscopy (FE-SEM) and UV–vis spectroscopy elucidated the rate of RB5 degradation.

2. Experimental details

2.1. Synthesis of iron oxide nanoparticles and carbon-based nanocomposites

The synthesis route of iron oxide nanospheres (IONS) was based on our previous work [43]. Here, the procedure was successfully applied to prepare iron oxide nanoparticles with spherical morphology. The nanoparticles were prepared by a two-step procedure, co-precipitation at room temperature followed by hydrothermal treatment in

a microwave field at 100 °C. Briefly, iron(II) and iron(III) salts (in molar ratio 1:2) were added to round bottom flasks under a blanket of nitrogen and strong mechanical stirring. The nanoparticles were precipitated with the addition of NH_4OH and transferred to a microwave reactor. The power of microwave irradiation was set between 0-1000 W, with a linear heating program from room temperature to 100 °C for 20 min Vessels were quickly cooled in an airflow, and the black product was collected by an external magnet, washed with demineralized water several times, and dried at 60 °C.

Multicore iron oxide nanoflowers (IONF) were obtained by polyol mediated reduction of iron(III) chloride. IONF were prepared as described in more detail elsewhere [44], but the experimental procedure, concentrations of iron(III) chloride and NaAc and reaction time were changed. In brief, 0.9 mmol of iron(III) chloride were ultrasonically dissolved in 109 mL of ethylene glycol. Then, 140 mmol of PVP40 were slowly added to prevent formation of lumps under vigorous magnetic stirring (1350 rpm) with mild heating until complete dissolution. After this, 15.8 mmol of NaAc was added to the solution. The mixture was sealed in a Teflon-lined stainless-steel autoclave of 150 ml capacity and transferred to the oven (Memmert UN55, Germany). The temperature of the system was maintained at 200 °C for 8 h for solvothermal crystallization, followed by cooling inside the oven. The supernatant was discarded and the dark brown precipitates were washed several times with ethanol *via* centrifugation (6163 RCF, Sorenson BioSense, Inc, USA) and finally dried overnight at 60 °C.

Synthesis procedures for iron oxide nanocubes (IONC) and iron oxide nanoneedles (IONN) were described in references [45] and [46], respectively.

The prepared nanoparticles described above were dispersed in dimethylformamide (DMF) in an ultrasonic bath and used for modification of the electrode surface. After selecting the best candidate for degradation of Reactive Black 5, the synthesized IONS were used to decorate various carbon-based materials with different carbon arrangements, i.e., graphene (GN), carboxylated graphene (cGN), graphene oxide (GO), graphene nanoribbons (GNR), graphene nanoplatelets (GNP), single-wall carbon nanotubes (SWCNT), and multi-wall carbon nanotubes (MWCNT), by mixing nanoparticles with carbon compounds in a 3:1 mass ratio and dispersing them in (DMF) in an ultrasound bath. Typically, 3 mg of INOP were mixed with 1 mg of carbon materials, dispersed in 1 ml of DMF, and sonicated for 3 h at room temperature, to form a uniform suspension. Concentration of IONP in the suspension was 3 mg ml^{-1}.

2.2. Electrode preparation

The screen-printed carbon electrodes were produced from carbon ink (No. C50905DI, Gwent, Pontypool, UK) and laser pre-etched ceramic supports (No. CLS 641000396 R, Coors Ceramics GmbH, Chattanooga, TN, USA). Thick layers of carbon ink were formed by brushing the ink through an etched stencil (thickness 100 μm, electrode printing area 100 mm^2) with the aid of a screen-printing device (SP-200, MPM, Franklin, MA, USA) onto the ceramic supports. The resulting plates were dried overnight at room temperature. Each modified screen-printed electrode was prepared by dropping 60 μl of synthesized composite on the electrode surface and allowing it to dry for 3 h.

Based on our previous experience, the experimental galvanic conditions for electrochemical removal of the selected dye, RB5, were standardized as follows: 0.05 M potassium chloride (KCl) as the supporting electrolyte; applied potential of 3 V, and; pH 2 achieved by addition of 0.01 M hydrochloric acid (HCl) [47].

2.3. Experimental methods

2.3.1. Characterization of the materials

Morphologies of synthesized materials and nanocomposites were examined using a field emission-scanning electron microscope FE-SEM MIRA3 (Tescan, Czech Republic) coupled with an EDS analyzer (Oxford, UK) and transmission electron microscopes JEOL-TEM 1010 (JEOL, Japan) operating at 100 kV and JEOL-TEM 2100 F at 200 kV. Diluted dispersions of IONP and nanocomposites were dropped on a carbon-coated copper grid and left to dry at room temperature for FE-SEM and TEM observations. The TEM images were analyzed by Image J software [48] in manual mode, and the mean particle sizes (d_{TEM}) were obtained by measuring the largest internal dimension of at least 100 particles. Afterwards, the data were fitted through Origin software to a log-normal function $\left(y = y_0 + \frac{A}{\sqrt{2\pi\omega x}} \exp \frac{-\left[\ln \frac{x}{x_c}\right]^2}{2\omega^2} \right)$ to obtain the mean size ($\overline{x}$) and the standard deviation (σ).

Crystal structures of the prepared materials were examined by X-ray powder-diffraction (XRD) performed on a high-resolution SmartLab® X-ray diffractometer (Rigaku, Japan) with CuKα radiation source and accelerating voltage of 40 kV and current 30 mA. Samples were prepared by flattening dried powders with a zero-background silicon wafer, and diffraction patterns were collected within 10-70° 2θ range. Mean crystallite size, d_{XRD}, was obtained by Scherrer's equation $d_{XRD} = \frac{K \cdot \lambda}{\beta \cdot \cos\theta}$, where constant K (assumed to be equal 0.9) is related both to the crystallite shape and to the definition on both β and d_{XRD}, λ is the x-ray wavelength, β is the full-width at half maximum of the particular diffraction peak. The d_{XRD} values were determined as averaged from the most intensive reflections.

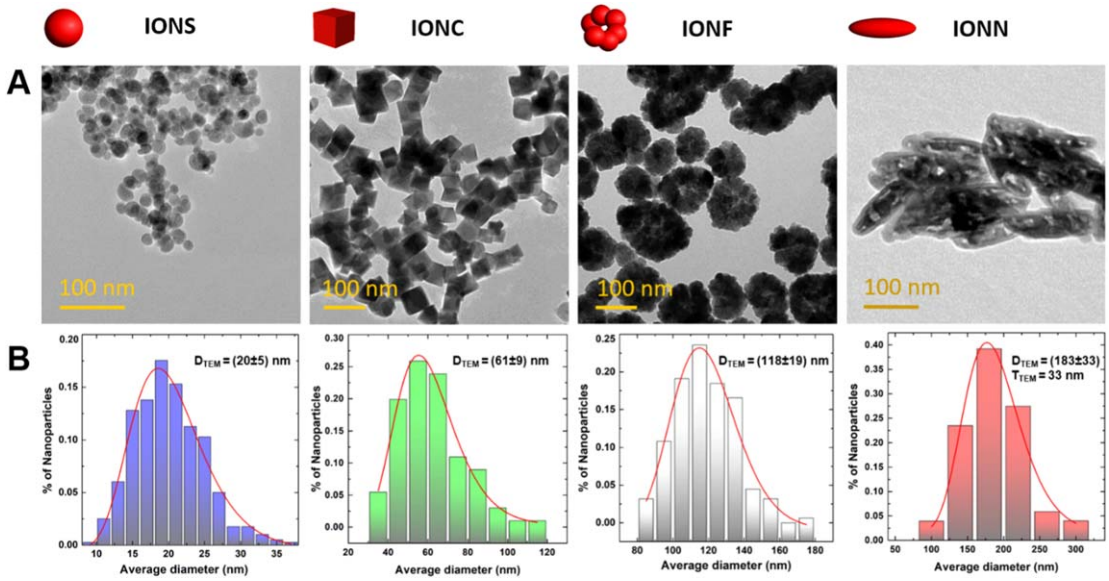

Figure 1. (A) Transmission electron microscopy (TEM) images of IONPs: iron oxide nanospheres (IONS, 20 nm), iron oxide nanocubes (IONC, 61 nm), iron oxide nanoflowers (IONF, 118 nm) and iron oxide nanoneedles (IONN, 183 nm), and; (B) Log-normal size distributions of the respective IONPs.

Magnetic measurements were carried out in a SQUID magnetometer MPMS 5XL, Quantum Design with a maximum field of 30 kOe. Each sample was dried in an inox-coated oven at 50 °C overnight. Afterwards, the samples were accurately weighed and fitted into the sample holder. A hysteresis loop of each powder sample was measured at 295 K at a rate of 0.5 kOe·min^{-1}. The saturation magnetization (M_S) was estimated by using the equation $M = M_s\left(1 - \frac{a}{H} - \frac{b}{H^2}\right)$ for H tending to ∞.

2.3.2. Electrocatalytic activity of the modified electrodes

RB5 degradation was studied in an undivided two-electrode cell containing 50 mL of 40 mg L^{-1} (ppm) of the dye, and equipped with unmodified (cathode) or modified screen-printed electrodes (anode) with an active area of 100 mm^2 (25 × 4 mm) as working electrodes. During all experiments, mild magnetic stirring was used to ensure the homogeneity of the solution. Experiments were carried out under galvanostatic conditions, with an adjustable laboratory DC power supply Hyelec HY3003 (0-30 V DC, 0-3 A). UV-Visible spectrophotometer (Evolution 200 Series, Thermo Fisher Scientific, Bremen, Germany) was used to monitor the decolourization rate at the maximum absorption wavelength $\lambda_{max} =$ 597 nm. A small amount of solution was taken out from the cell every 5 min until complete discolouration occurred.

3. Results and discussion

3.1. Structural and magnetic characterization of IONPs

Differently shaped IONPs were thoroughly characterized to determine their microstructural (morphology and particle/crystallite size) and magnetic (saturation magnetization and coercive field) properties, in order to ascertain which would be suitable for electrode surface modification.

The morphologies of the IONPs were investigated by TEM. Figure 1(A) and figure S1 is available online at stacks.iop.org/MRX/7/015509/mmedia (supplementary material) show representative TEM micrographs of IONPs with different morphologies (IONS, IONC, IONF and IONN). Iron oxide nanospheres (IONS) were pseudo-spherically shaped, partially aggregated with mean diameter of 20 (±5) nm. The morphology of cube-like nanoparticles (IONC) was mostly octahedral or cubic, and they were aggregated forming chains and fractal structures with mean diameter of 61 (±9) nm. Iron oxide nanoflowers (IONF) were composed of spherical, log-normally distributed multicore nanoparticles with a mean diameter of 118 (±19) nm, with well-defined size and shape [47]. These flower-like nanoparticles consisted of smaller cores of approximately 15 nm. The cores were densely packed, forming particles of characteristic size and shape resembling a flower. Iron oxide nanoneedles (IONN) had a mean length of 183 (±33) nm with an axial ratio of 5.5. The mean diameters of the nanoparticles (d_{TEM}) and polydispersity (given in percentage; σ_{TEM}) are listed in table 1. Figure 1(B) reveals the log-normal distributions of nanoparticles with different morphologies.

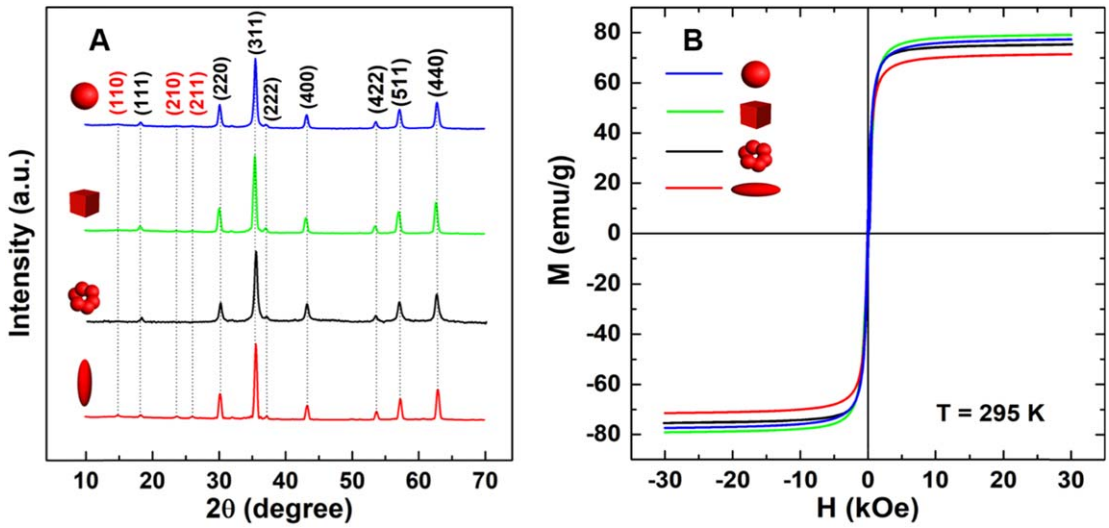

Figure 2. (A) XRD patterns of differently shaped IONP obtained by CuKα source and; (B) Hysteresis loops of IONP at RT.

Table 1. Particle size (d_{TEM}), polydispersity (σ_{TEM}), crystallite size (d_{XRD}), lattice parameter (a) and saturation (M_S) magnetization of different morphologies of IONP.

IONP	d_{TEM} (nm)	σ_{TEM}(%)	d_{XRD} (nm)	a (Å)	M_s (emu/g)
IONS	19.8	26.1	15.5(3)	8.368(7)	77.3
IONC	59.2	26.2	58.9(1)	8.392(3)	78.1
IONF	117.7	15.7	20.9(7)	8.397(4)	75.3
IONN	185.2	21.6	27.0(2)	8.372(2)	71.4

The XRD patterns of the IONPs are shown in figure 2(A). All of the reflections for samples IONS, IONC and IONF were assigned and indexed in agreement with the JCPDS PDF Card #19-629 in the Fd-3m (No. 227) space group of the cubic structure, and indicated that the synthesized nanoparticles being magnetite (Fe_3O_4). In the diffraction pattern of IONN it was noticed three small reflections of appearing at 15°, 23.9 ° and 26.2°, which can be ascribed to the (110), (210) and (211) reflections of maghemite (γ-Fe_2O_3) phase, and therefore it can be concluded that IONN nanoparticles crystallize in $P4_332$ space group (JCPDS PDF Card #96-230-0618, [49]). However, on the nanoscale, by analysing diffraction patterns it is very difficult to distinguish differences in maghemite (γ-Fe_2O_3) and magnetite (Fe_3O_4) crystal structure. Probably, in the most synthesised samples, there is a mixture of magnetite and maghemite phases with a different ratio. In all diffraction patterns, it was noticed a small reflection at 32.8° coming from the hematite phase (Fe_2O_3), but intensities of these reflections are negligible. The crystallite sizes determined by Sherer's formula, d_{XRD}, agree well with d_{TEM} in the case of IONS ($d_{XRD} =$ 15.5 nm) and IONC ($d_{XRD} =$ 58.9 nm), and are comparable with the core size of IONF ($d_{XRD} =$ 20.9 nm), but are significantly smaller than the particle sizes. This reflects the multicore nature of each nanomaterial. In the case of IONN, d_{TEM} denoted the length of the needles (183 nm).

Figure 2(B) presents the hysteresis loops of the four different morphology types of IONP: IONS, IONC, IONF and IONN at 295 K, and table 1 summarizes the saturation magnetization (M_S), remnant magnetization (M_R) and coercivity (H_C). All the magnetization curves pass through the origin in the magnetization graphs (Hc, $M_R \sim 0$ Oe), which means the synthesized nanoparticles are superparamagnetic at room temperature. The saturation magnetization ranged from 78.1 emu g^{-1} for IONC to 71.4 emu g^{-1} for IONN, which are common literature values for magnetite or maghemite nanoparticles [50].

3.2. Electrochemical impedance spectroscopy measurements

Electrochemical impedance spectroscopy (EIS) was used to confirm the interference properties of the fabricated electrodes before and at each modification step and to further characterize IONP, nanocomposites, and electrodes (figure 3). The impedance spectra contained a semi-circular part at higher frequencies corresponding to the electron-transfer resistance (R_{et}) and a linear part at lower frequencies belonging to the diffusion-limited process [51]. EIS measurements in the frequency range from 1×10^5 to 0.1 Hz using modified SPCE with differently shaped IONPs (figure 3(A)) indicate that modifying the electrode surface with the synthesized IONPs

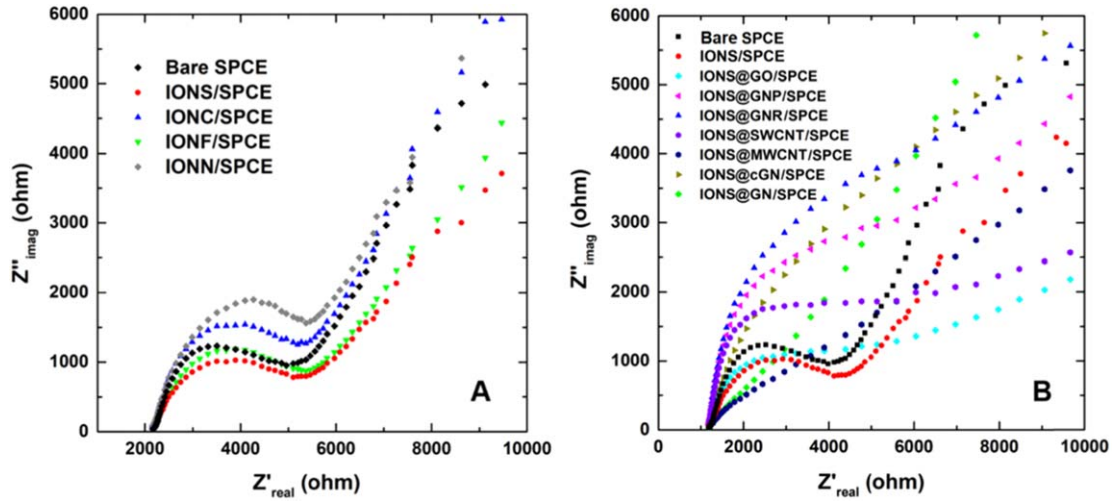

Figure 3. EIS spectra of the modified electrodes with A) IONPs with different morphologies, and; B) composite IONS@carbon-based materials.

was followed by decrease of the semicircle diameters in Nyquist plots. Here, the lowest diameter was obtained with IONS-modified SPCE, which can be explained by the greater active surface area and better conductivity of the modified electrode compared to the bare electrode. This is beneficial for interfacial properties between test solutions and electrode and should enhance the transportation of electrochemically-produced charges at the solution/electrode interface. IONS were then selected to modify different carbon-based materials, thus making nanocomposites (IONS@CBM). EIS spectra of IONS@CBM-modified SPCE electrodes (figure 3(B)) showed that some combinations of the carbon materials (MWCNT, GN, GO) have impedance spectra with semicircle diameters that were barely observable. This suggests impedance can be ignored, because MWCNT, GN and GO had outstanding electroconductivity, which should enhance the electron transfer and thus hold smaller resistance, while the resistance values gradually increased up to that of SWCNT. Additionally, GN and MWCNT produced the widest range of linear measurements, indicating diffusion-controlled processes.

3.3. Comparative study of decolourization of Reactive Black 5 by bare SPCE and IONP-modified screen-printed electrodes

In the above studies, it was proven that the modification procedure improved the electrochemical characteristics of the SPCE electrode surface. However, the efficiency of modified and unmodified electrodes in the removal of a dye was not yet clear, so this was examined using 50 mg l^{-1} RB5. Results are summarized in figure 4(A). With bare SPCE, after 61 min of electrolysis, colour removal was around 95%, while modifying the electrode with IONP (IONP/SPCE) increased the dye removal efficiency up to 99% after 51 min of treatment. This resulted in a 15% saving of time and energy consumption. It can be deduced the electrode efficiency was strongly correlated with size and morphology of nanoparticles because IONS had the smallest diameter which resulted in the highest surface area, followed by IONF, which are composed of smaller cores that best degrade RB5. This was also confirmed by EIS, showing the greater active surface area achieved by electrode modification. Figure 4(B) shows that by increasing the reaction time, the intensity of the $\lambda = 597$ nm band decreased. The reduction in the 597 nm absorption band was most likely due to hydrogenation of azo bonds and conversion of –N = N– to $-NH_2$ that breaks the long conjugated π-system of RB5 [52] and produces the small aromatic amines and sulfanilic acid derivatives characteristic of RB5 degradation [53]. The effect of iron oxide nanoparticles on –N = N– bonds is well known and reported [54], so the mechanism of this degradation was not further explored. In the next step, the material with the best decolourizing performance (IONS) was chosen to decorate various carbonaceous materials, to further improve the electrode surface.

3.4. Comparative study of decolourization of Reactive Black 5 by bare SPCE and IONP modified screen-printed electrodes

Different IONS@CBM nanocomposites were used to modify SPCE electrodes.

3.4.1. Electrocatalytic activity of the proposed method

A comprehensive overview of electrochemical removal of RB5 measured with UV-Vis spectroscopy, and improvements to the time needed for complete (~99%) decolourization of RB5 are given in figure 5. The best

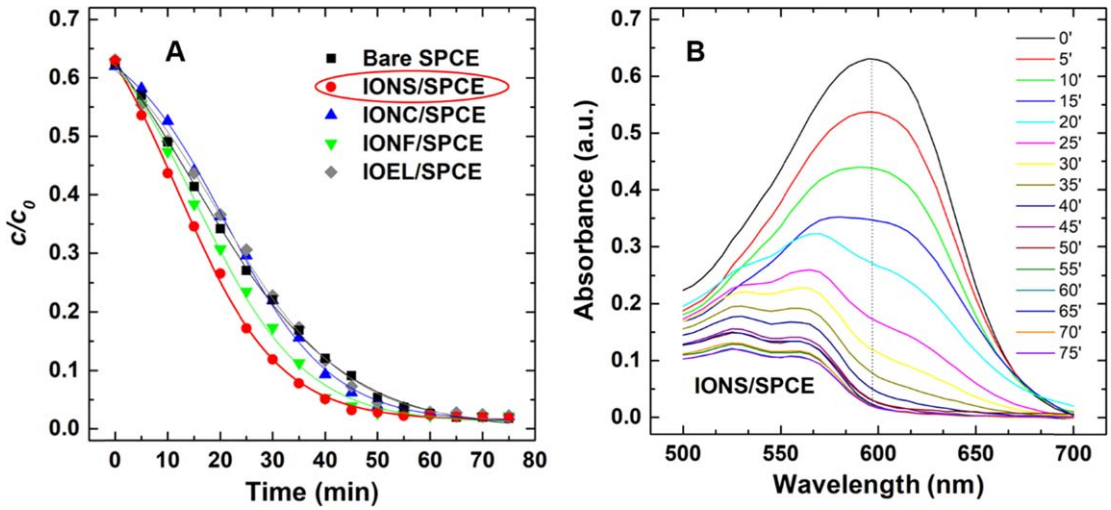

Figure 4. (A) Electrochemical removal of RB5 with IONP-modified SPCE, and; (B) Absorbance of IONS/SPCE at $\lambda = 597$ nm in 5 min intervals up to 75 min.

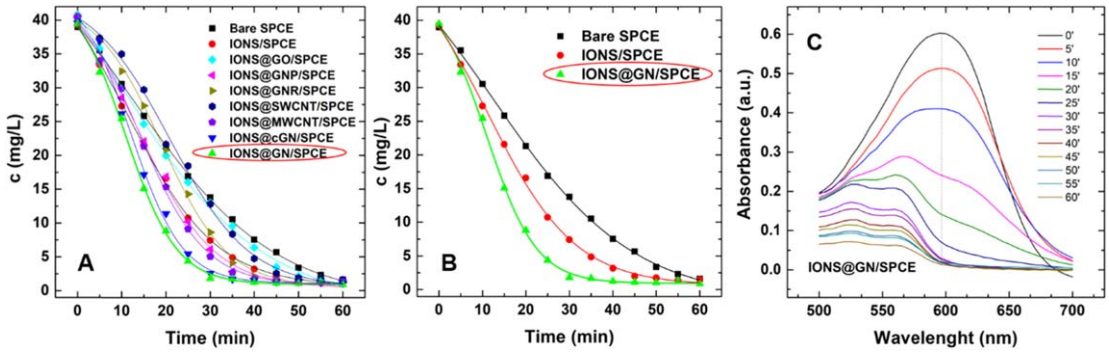

Figure 5. Electrochemical removal of Reactive Black 5 using IONS@carbon-based materials for SCPE modification: (A) degradation performance with different carbon-based materials to modify SPCE; (B) Improvement of degradation performance using modified electrodes, and; (C) Absorbance of IONS@GN/SPCE over a period of 75 min

efficiency was achieved with IONS@GN/SPCE (iron oxide nanospheres on graphene/screen-printed carbon electrode), with which ~99% of dye was removed from water in only 31 min, a 51% improvement compared to the bare electrode, as shown in figure 5(A). In figure 6(B), the dye removal is depicted, showing improving effectiveness in the order from worst to best: bare SPCE < IONS-modified SPCE < IONS@GN-modified SPCE. Thus, the modified electrodes significantly increased the dye degradation rate over that of bare SPCE. In figure 5(A), the improvement of dye decolourization after decoration of different carbon-based materials is displayed. It can be noted that most of the carbon-based nanocomposites had a similar or better ability to decolourize the dye as did bare SPCE. Only GO and SWCNT decorated with IONS resulted in slower degradation rates than the pure IONS/SPCE electrode. These results are in good agreement with the results of EIS. Specifically, GN and MWCNT had the best EIS spectra, as described earlier (section 3.2; figure 3). Almost complete omission of semicircle diameter in the Nyquist plot was observed, indicating the larger electrode active area and better conductivity, and greatest linear ranges occurred at lower frequencies; this would enhance diffusion. In figure 6(C), absorbance spectra of IONS@GN/SPCE over a 75 min period is given, showing that complete degradation of the peak at 597 nm occurred after only 30 min.

3.4.2. Characterisation of the IONS@CBM composite

Typical FE-SEM images of IONS decorated on carbon-based materials (IONS@CBM) are shown in figure 6. IONS are uniformly dispersed on top of the carbonaceous materials, increasing the surface areas of the electrodes. This is beneficial for interfacial properties between the dye solution and electrode and enhances transport of electrochemically produced charges at the solution/electrode interfaces, which is crucial for dye removal.

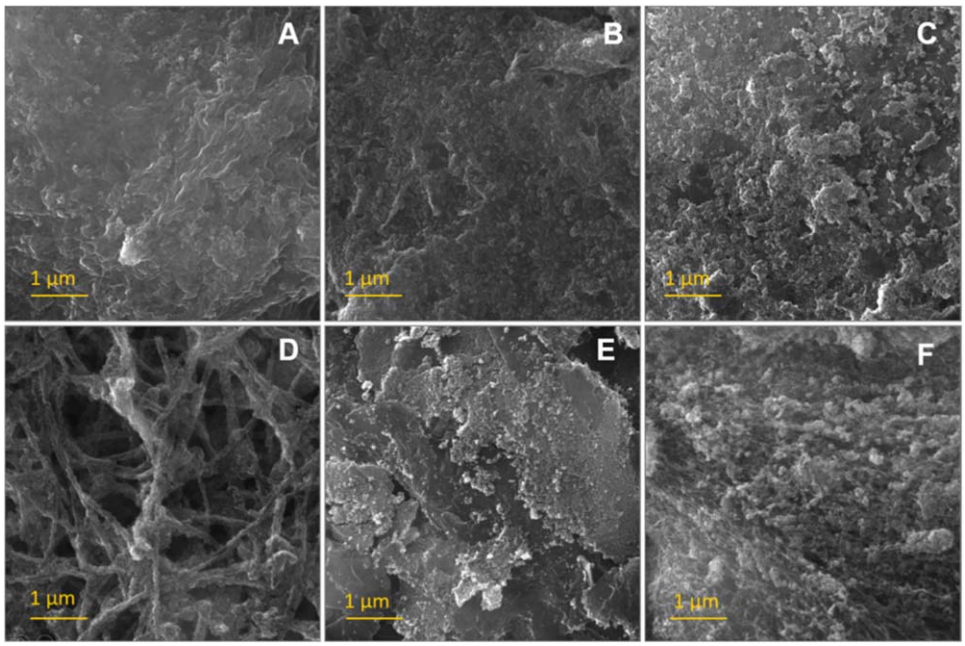

Figure 6. FE-SEM microscopy of: (A) IONS decorated on carboxylated graphene (ION@cGN); (B) IONS decorated on graphene (ION@GN); (C) IONS on graphene oxide (ION@GO); (D) IONS on graphene nanoribbons (ION@GNR); (E) IONS on graphene nanoplatelets (ION@GNP), and; (F) IONS on multi-wall carbon nanotubes (ION@MWCNT).

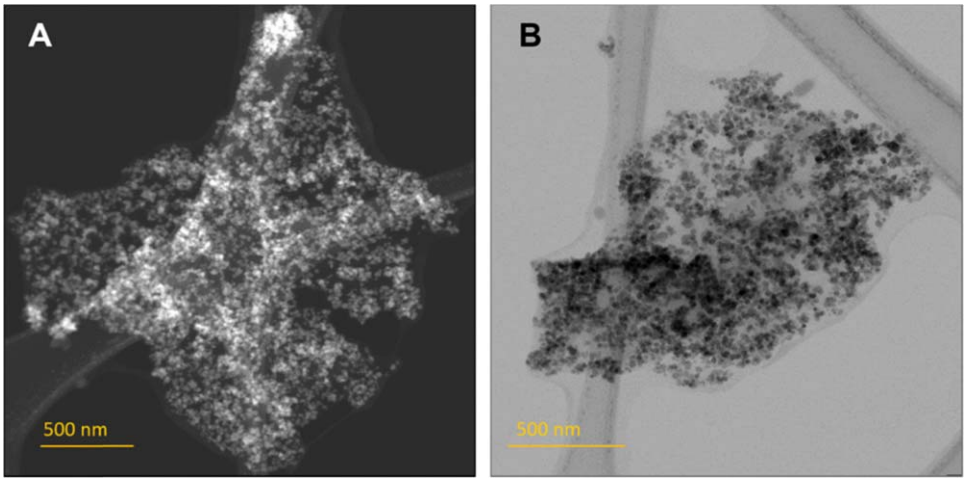

Figure 7. TEM micrographs of IONS@GN (A) Dark-field; (B) Bright-field microscopy recorded by JEOL-TEM 2100 F.

Figure 7 shows TEM micrographs of nanocomposite IONS@GN, which had the best dye removal efficiency after modification of SCPE (among the examined materials), revealing highly dispersed small spherical nanoparticles decorated over the whole surface of GN. GN is an almost transparent thin-film possessing desirable properties for anchoring small IONS. GN's large number of wrinkles and folds provided a larger surface area than the other materials, and subsequent better conductivity after it was decorated with the IONS. This finally resulted in the finished IONS@GN/SPCE electrode having the highest RB5 removal efficiency among all the electrodes we constructed.

The results of our research are summarized in figure 8, schematically displaying the rates of RB5 degradation we achieved by modifying the SPCE surface using IONPs with different morphologies (figure 8(A)), and the rates we achieved after decorating some commonly used carbon-based materials (figure 8(B)). It can be concluded that the performance of SPCE in degrading the organic dye was significantly improved by this electrochemical approach. Specifically, a 51% performance increase over the other carbon-based materials used was achieved using the combination of IONS decorated on graphene to modify SPCE.

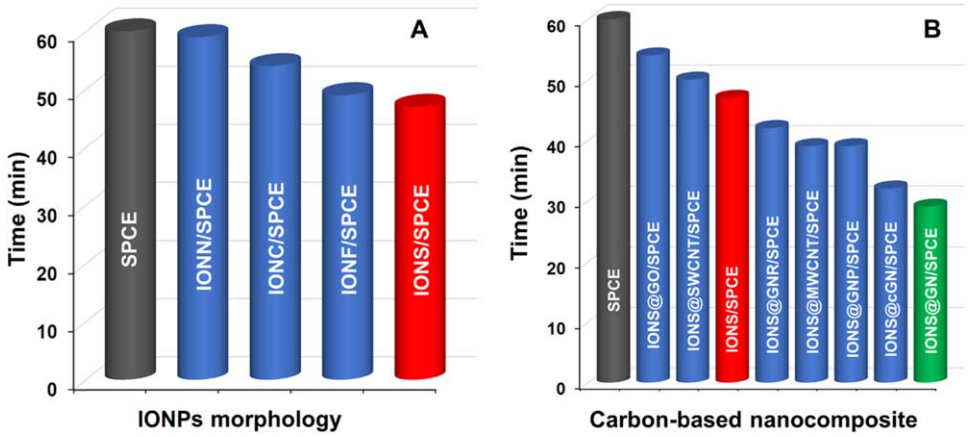

Figure 8. Summary of efficiency of electrochemical removal of Reactive Black 5 using (A) modified SPCE with differently shaped IONP, and; (B) IONS decorated on various carbon-based materials.

4. Summary

It was demonstrated that using different synthesis methods, the desired morphology of nanoparticles can be fine-tuned. The ability of SPCE to degrade the organic dye RB5 is significantly improved by deposition of IONP on the electrode surface. Among the electrodes constructed, the best results were achieved by modifying SPCE with spherical IONP (IONS), as this electrode removes 99% of the dye in 51 min, a performance improvement of 16% over bare SPCE. After selecting the best IONP (i.e., spherical) for SPCE modification, the synthesized IONS were decorated onto various carbon-based materials with different carbon arrangements: graphene (GN), carboxylated graphene (cGR), graphene oxide (GO), graphene nanoribbons (GNR), graphene nanoplatelets (GNP), single-wall carbon nanotubes (SWCNT) and multi-wall carbon nanotubes (MWCNT). The nanocomposites formed were then used to modify SPCE in order to enhance the efficiency of electrochemical degradation of the azo dye, RB5. Using the same, standard galvanic conditions, results show the combination of IONS@GN/SPCE provides the best outcome, effecting complete removal of the dye in just over 30 min, so this electrode is 51% more efficient than the bare electrode. These results were very consistent with EIS and electron microscopy results. Overall, the performance improvement can be explained by the greater active surface area and better conductivity of the modified electrode, making it more conducive for the transportation of electrochemically produced charges at the solution/electrode interface.

Acknowledgments

The authors like to thank Prof. M.P. Morales for providing samples of IONC and IONN used in this study. This work was supported through the European Commission by MagBioVin project (FP7-ERA Chairs-Pilot Call-2013, Grant agreement: 621375), Ministry of Education, Science and Technological Development of the Republic of Serbia (Projects No. OI 172030, III45015 and E9982!). MF wishes to acknowledge the APVV (Project No. SK-SRB-18-0055).

ORCID iDs

Miloš Ognjanović https://orcid.org/0000-0003-2889-4416
Antić Bratislav https://orcid.org/0000-0002-5693-6401

References

[1] Revia R A and Zhang M 2016 *Materials today (Kidlington, England)* **19** 157–68
[2] Mohammed L, Gomaa H G, Ragab D and Zhu J 2017 *Particuology* **30** 1–14
[3] Duan M, Shapter J G, Qi W, Yang S and Gao G 2018 *Nanotechnology* **29** 452001
[4] Wan Z, Zhang G, Wang J and Zhang Y 2013 *RSC Adv* **3** 19617
[5] Wen Z, Zhang Y, Dai C and Sun Z 2015 *Journal of hazardous materials* **287** 225–33
[6] Guo Y, Zhang G, Liu J and Zhang Y 2013 *RSC Adv* **3** 2963
[7] Zhang G, Gao Y, Zhang Y and Guo Y 2010 *Environmental science & technology* **44** 6384–9
[8] Zhang Y, Deng L, Zhang G and Gan H 2011 *Colloids and Surfaces A: Physicochemical and Engineering Aspects* **384** 137–44

[9] Zhang Y, Gan H and Zhang G 2011 *Chemical Engineering Journal* **172** 936–43
[10] Zhang Y, Wang D and Zhang G 2011 *Chemical Engineering Journal* **173** 1–10
[11] Wang Y, Zhang Y-n, Zhao G, Wu M, Li M, Li D, Zhang Y and Zhang Y 2013 *Separation and Purification Technology* **104** 229–37
[12] Li D, Zhang Y, Zhang Y, Zhou X and Guo S 2013 *Journal of hazardous materials* **258-259** 42–9
[13] Madhuvilakku R, Alagar S, Mariappan R and Piraman S 2017 *Sensors and Actuators B: Chemical* **253** 879–92
[14] Patnaik S, Martha S, Acharya S and Parida K M 2016 *Inorganic Chemistry Frontiers* **3** 336–47
[15] Sham A Y W and Notley S M 2013 *Soft Matter* **9** 6645–53
[16] Zhu J, Yang D, Yin Z, Yan Q and Zhang H 2014 *Small* **10** 3480–98
[17] Zhang Y, Li D, Zhang Y, Zhou X, Guo S and Yang L 2014 *J. Mater. Chem.* A **2** 8273–80
[18] Justino C I L, Gomes A R, Freitas A C, Duarte A C and Rocha-Santos T A P 2017 *TrAC Trends in Analytical Chemistry* **91** 53–66
[19] Kuila T, Bose S, Mishra A K, Khanra P, Kim N H and Lee J H 2012 *Progress in Materials Science* **57** 1061–105
[20] Ziółkowski R, Górski Ł and Malinowska E 2017 *Sensors and Actuators B: Chemical* **238** 540–7
[21] Higginbotham A L, Lomeda J R, Morgan A B and Tour J M 2009 *ACS applied materials & interfaces* **1** 2256–61
[22] Uhl F M and Wilkie C A 2004 *Polymer degradation and Stability* **84** 215–26
[23] Luo J, Shen P, Yao W, Jiang C and Xu J 2016 *Nanoscale research letters* **11** 141
[24] Ognjanović M, Stanković D M, Fabián M, Vukadinović A, Prijović Ž, Dojčinović B and Antić B 2018 *Electroanalysis* **30** 2620–7
[25] Aguilar-Bolados H, Lopez-Manchado M A, Brasero J, Avilés F and Yazdani-Pedram M 2016 *Composites Part B: Engineering* **87** 350–6
[26] Hashemi P, Bagheri H, Afkhami A, Amidi S and Madrakian T 2018 *Talanta* **176** 350–9
[27] Nguyen H N, Castro-Wallace S L and Rodrigues D F 2017 *Environ. Sci.: Nano* **4** 160–9
[28] Tang W-W, Zeng G-M, Gong J-L, Liu Y, Wang X-Y, Liu Y-Y, Liu Z-F, Chen L, Zhang X-R and Tu D-Z 2012 *Chemical Engineering Journal* **211** 470–8
[29] Simate G S, Iyuke S E, Ndlovu S and Heydenrych M 2012 *Water Research* **46** 1185–97
[30] Teymourian H, Salimi A and Khezrian S 2013 *Biosensors & bioelectronics* **49** 1–8
[31] Wang Y, Zhao H, Gao J, Zhao G, Zhang Y and Zhang Y 2012 *J. Phys. Chem.* C **116** 7457–63
[32] Guo Y, Zhang G, Gan H and Zhang Y 2012 *Dalton transactions (Cambridge, England : 2003)* **41** 12697–703
[33] Vanraes P *et al* 2015 *Journal of hazardous materials* **299** 647–55
[34] Zheng Y, Yao G, Cheng Q, Yu S, Liu M and Gao C 2013 *Desalination* **328** 42–50
[35] Alventosa-deLara E, Barredo-Damas S, Alcaina-Miranda M I and Iborra-Clar M I 2012 *Journal of hazardous materials* **209** 492–500
[36] Garg S K, Tripathi M, Singh S K and Tiwari J K 2012 *International biodeterioration & biodegradation* **74** 24–35
[37] Amani-Ghadim A R, Aber S, Olad A and Ashassi-Sorkhabi H 2013 *Chemical Engineering and Processing: Process Intensification* **64** 68–78
[38] Rosales E, Pazos M and Sanromán M A 2011 *Desalination* **278** 312–7
[39] Vahid B and Khataee A 2013 *Electrochimica Acta* **88** 614–20
[40] Del Río A I, Fernández J, Molina J, Bonastre J and Cases F 2011 *Desalination* **273** 428–35
[41] Afkhami A and Norooz-Asl R 2009 *Colloids and Surfaces A: Physicochemical and Engineering Aspects* **346** 52–7
[42] Ngomsik A-F, Bee A, Draye M, Cote G and Cabuil V 2005 *Comptes Rendus Chimie* **8** 963–70
[43] Ognjanović M, Dojčinović B, Fabián M, Stanković D M, Mariano J F and Antić B 2018 *Ceramics International* **44** 13967–72
[44] Gavilán H, Sánchez E H, Brollo M E F, Asín L, Moerner K K, Frandsen C, Lázaro F J, Serna C J, Veintemillas-Verdaguer S and Morales M P 2017 *ACS Omega* **2** 7172–84
[45] Vergés M A, Costo R, Roca A G, Marco J F, Goya G F, Serna C J and Morales M P 2008 *Journal of Physics D: Applied Physics* **41** 134003
[46] Gavilán H, Posth O, Bogart L K, Steinhoff U, Gutiérrez L and Morales M P 2017 *Acta Materialia* **125** 416–24
[47] Stanković D M, Ognjanović M, Espinosa A, del Puerto Morales M, Bessais L, Zehani K, Antić B and Dojcinović B 2019 *Electrocatalysis* **10** 663–71
[48] Schneider C A, Rasband W S and Eliceiri K W 2012 *Nature methods* **9** 671
[49] Solano E, Frontera C, Puig T, Obradors X, Ricart S and Ros J 2014 *J Appl Crystallogr* **47** 414–20
[50] Teja A S and Koh P-Y 2009 *Progress in Crystal Growth and Characterization of Materials* **55** 22–45
[51] Zhang X, Li F, Wei Q, Du B, Wu D and Li H 2014 *Sensors and Actuators B: Chemical* **194** 64–70
[52] Nam S and Tratnyek P G 2000 *Water Research* **34** 1837–45
[53] Hou M, Li F, Liu X, Wang X and Wan H 2007 *Journal of hazardous materials* **145** 305–14
[54] Samiee S, Goharshadi E K and Nancarrow P 2016 *Journal of the Taiwan Institute of Chemical Engineers* **67** 406–17